ACS chemical biology

Articles

pubs.acs.org/acschemicalbiology

Structure of Mycobacterial β-Oxidation Trifunctional Enzyme Reveals Its Altered Assembly and Putative Substrate Channeling Pathway

Rajaram Venkatesan and Rik K. Wierenga*

Department of Biochemistry and Biocenter Oulu, University of Oulu, Oulu 90014, Finland

Supporting Information

ABSTRACT: The incidence of tuberculosis is increasing due to the appearance of new drug-resistant variants. A thorough understanding of the disease organism is essential in order to create more effective drugs. In an attempt to understand better the poorly studied lipid metabolism of *Mycobacterium tuberculosis* (Mtb), we identified and characterized its fatty acid β-oxidation complex (trifunctional enzyme (TFE)). TFE is an $\alpha_2\beta_2$ complex consisting of two types of polypeptides catalyzing three of the four reactions of the β-oxidation of fatty acids. The kinetic constants (k_{cat} and K_m) show that the complexed α chain is more active than the individual α chain. Crystal structures of Mtb TFE (mtTFE) reveal that the quaternary assembly is strikingly different from the already known *Pseudomonas fragi* TFE (pfTFE) assembly due to the presence of a helical insertion (LA5) in the mtTFE-β subunit. This helical insertion prevents the pfTFE mode of assembly, as it would clash with helix H9A of the TFE-α chain. The mtTFE assembly appears to be more rigid and results in a different substrate channeling path between the α and the β subunits. Structural comparisons suggest that the mtTFE active sites can accommodate bulkier fatty acyl chains than in pfTFE. Although another thiolase (FadA2), more closely related to human TFE-β/thiolase, is present in the Mtb genome, it does not form a complex with mtTFE-α. Extensive phylogenetic analyses show that there are at least four TFE subfamilies. Our studies highlight the molecular properties of mtTFE, significantly extending the structural knowledge on this type of very interesting multifunctional enzymes.

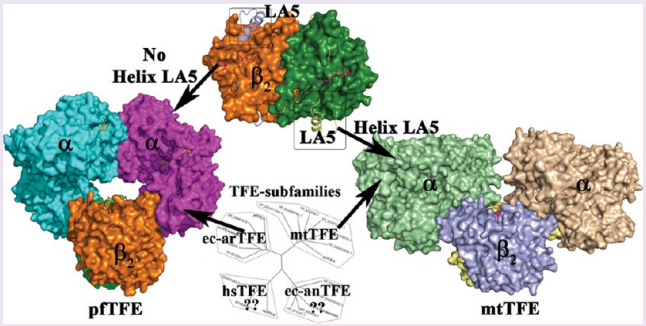

Mycobacterium tuberculosis (Mtb) is the causative agent of the deadly disease tuberculosis.[1] Worldwide it accounts for approximately 1.4 million deaths annually. The incidence of the disease is increasing in developing as well as developed countries also because of the appearance of drug-resistant strains.[2] In the intracellular stage, the survival of Mtb depends on the degradation of host-derived fatty acids, which are more important as a nutrient than the host carbohydrates.[3−5] The importance of the Mtb lipid metabolism is consistent with the notion that a surprisingly large number of genes of the Mtb genome code for enzymes involved in lipid metabolism;[6−8] for example, more than 250 genes code for enzymes involved in fatty acid metabolism.[6] The Mtb lipid metabolism is poorly characterized. Structural enzymology approaches are essential for a better understanding of the enzymes involved in this metabolism. Such knowledge will also greatly facilitate drug discovery research for combating the deadly disease caused by Mtb.

The focus of our research concerns the enzymes of the β-oxidation pathway of Mtb by which fatty acids are degraded, once being conjugated to CoA. The thioester bond between the fatty acid and CoA activates the fatty acyl moiety for the subsequent conversions. A common feature in each of these reactions is therefore the thioester chemistry of the respective active sites.[9] In each of these active sites the thioester carbonyl oxygen is bound in an oxyanion hole.[10,11] The β-oxidation pathway consists of four steps, being (i) an acyl-CoA dehydrogenation, (ii) an enoyl-CoA hydration, (iii) a 3-hydroxyacyl-CoA dehydrogenation, and (iv) a thiolytic cleavage reaction (Figure 1). These reactions are catalyzed by monofunctional and multifunctional enzymes. The monofunctional enzymes of each of the four classes are well studied,[12] whereas the multifunctional enzymes are not. Trifunctional enzyme (TFE) is an important component of the β-oxidation pathway. As the name suggests, three different active sites are present in TFE, in which the α-subunit is homologous to multifunctional enzyme type 1 (MFE1) and the β-subunit is a thiolase. Bacterial TFE is a soluble $(\alpha_2\beta_2)$-complex, whereas the mammalian mitochondrial homologue is a membrane-associated $(\alpha_2\beta_2)$ dimer.[8,13] The best studied bacterial TFEs are from *Escherichia coli*[14] and from *Pseudomonas fragi* (pf).[15] The latter enzyme has been shown to have preferred substrate specificity for long chain fatty acid tail CoA substrate molecules.[16] The crystal structure of the pfTFE complex is known in different liganded states. The core of this assembly is the β_2 dimer, corresponding to a thiolase dimer, which is complexed with an α_2 dimer.[15]

Received: January 3, 2013
Accepted: March 15, 2013
Published: March 15, 2013

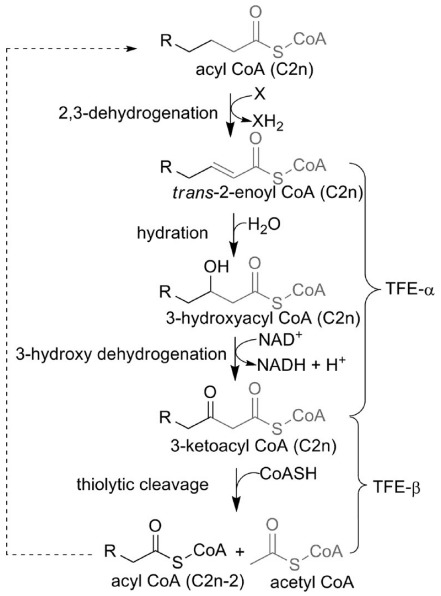

Figure 1. The four thioester-dependent reactions of the β-oxidation pathway. The second and third reactions are catalyzed by TFE-α, and the fourth reaction is catalyzed by TFE-β.

Substrate channeling is an interesting feature of multifunctional enzymes. In multifunctional enzymes,[17] the substrates can be channeled either by molecular tunneling[18,19] or by surface crawling[20] from one active site to the other active site without being released into the bulk solvent. Studies of the mitochondrial fatty acid β-oxidation systems strongly suggest the presence of substrate channeling,[21] but only few studies on the molecular enzymology of this complex have been done.[13,22,23] The substrate channeling of the bacterial TFEs have been studied only for the *E. coli* enzyme.

In this study we have characterized the Mtb TFE (mtTFE). The crystal structure is solved in the apo form as well as in its CoA-bound form, and the structural data have been complemented by enzymological and bioinformatics studies. It is found that the assembly of the Mtb complex is strikingly different from that of pfTFE.[15] The biochemical studies show that it accepts *trans*-2-decenoyl-CoA as its substrate and that the α chain of the complex is more active than the individual α-subunit. Sequence analyses show that there are at least four TFE subfamilies with mtTFE forming a new, previously unknown subfamily.

RESULTS AND DISCUSSION

In Mtb, the genes FadA and FadB occurring in a single operon have been identified to code for TFE-β and TFE-α chains, respectively. These two genes were cloned and coexpressed in *E. coli*. Static light scattering (SLS) studies on the purified mtTFE-α chain and mtTFE complex show that they are monomers (78 kDa) and $\alpha_2\beta_2$ tetramers (240 kDa) in solution, respectively.

Enzyme Activity. The enzymatic activities of each of the three active sites were characterized with *trans*-2-decenoyl-CoA as the substrate. This substrate is converted to 3-hydroxydecanoyl-CoA at the hydratase active site. The K_m and k_{cat} values for this reaction (Table 1) were determined as 15.3 ± 3.5 μM and 380.7 ± 39.1 s^{-1}, respectively, for the mtTFE complex. For the separate mtTFE-α chain, the K_m is 17.6 ± 1.6 μM, whereas k_{cat} is 173.2 ± 39 s^{-1}, which is two times lower as

Table 1. Kinetic Data Determined for mtTFE and mtTFE-α with *trans*-2-Decenoyl CoA as the Substrate

	hydratase	dehydrogenase
	mtTFE	
K_m (μM)	15.3 ± 3.5	1.7 ± 0.13
k_{cat} (s^{-1})	380.7 ± 39	10.27 ± 0.23
k_{cat}/K_m (10^6 M^{-1} s^{-1})	25.7 ± 5.4	6.2 ± 0.37
	mtTFE-α	
K_m (μM)	17.6 ± 1.6	5.8 ± 0.93
k_{cat} (s^{-1})	173.2 ± 39	2.8 ± 0.35
k_{cat}/K_m (10^6 M^{-1} s^{-1})	10 ± 3	0.49 ± 0.08

for the complex. The HAD reaction (L-3-hydroxyacyl-CoA dehydrogenase) is initiated by including NAD^+, which converts the 3-hydroxy-decanoyl CoA obtained from the hydratase active site to a 3-keto product. The K_m and k_{cat} values for the complex are 1.7 ± 0.1 μM and 10.3 ± 0.2 s^{-1}, respectively, whereas for the separate α chain the values are 5.7 ± 0.9 μM and 2.8 ± 0.4 s^{-1}, respectively (Table 1). As for the hydratase reaction, the k_{cat} of the HAD reaction of the separate α chain is significantly lower than that of the complex. The high k_{cat}/K_m values show the high catalytic efficiencies of both active sites of the α chain, in particular when assembled into the $\alpha_2\beta_2$-complex. Addition of CoA to the assay mixture of the complex initiates the thiolase degradative reaction and results in the formation of octanoyl-CoA and acetyl-CoA. The rate of the thiolase reaction of the complex is 24.5 ± 2.2 s^{-1} following the protocol as described in the Methods section. The presence of CoA in the reaction mixtures increases the HAD activity for mtTFE but not for the separate mtTFE-α, probably because in mtTFE the HAD product immediately transfers to the thiolase active site. The kinetic data confirm that each of the three active sites are active toward the degradation of this long chain acyl-CoA molecule.

Structural Studies. The $\alpha_2\beta_2$-complex was crystallized in its apo form, and a data set at 2.3 Å resolution was collected at the ESRF (Table 2). In addition, isomorphous crystals were obtained in the presence of 2 mM CoA. From the crystals of these CoA complexes two data sets were collected at 2.6 and 2.5 Å resolution, respectively (Table 2). In these crystals the asymmetric unit is an $\alpha_2\beta_2$-tetramer. The two α chains are referred to as subunits A and B, whereas the two β chains are referred to as subunits C and D. For the detailed analysis of the structure the A-subunit (α chain/MFE1) and the D-subunit (β chain/thiolase) of the 2.3 Å apo structure were used. The used secondary structure nomenclature follows previous conventions (Supplementary Figure S1, Supplementary Figure S2).

Structure of the mtTFE-α Chain. The α-subunits show continuous electron density from residue 1 to 720 in both chains. The overall structure of the α chain is similar to the peroxisomal monomeric MFE1 of rat[24] and plant[25] and the α chain of the pfTFE complex.[15] Likewise five domains (A, B, C, D, and E) have been identified (Figure 2A,B). The A-domain together with the B-domain forms the hydratase (crotonase) fold. The domains C, D, and E form the HAD fold. The B-domain is also described as the helix 10 (H10)[24] or the linker helix[15] between the hydratase fold and the HAD fold. The D/E domains form one tight structural unit. The two α-subunits of the $\alpha_2\beta_2$ tetramer superpose very well on each other. The only difference between the two subunits is the region of residues 548−579 in domain D, being helix DH3 and DH4, followed by the "HAD-specificity loop".[24] In subunit A, this region is more

dx.doi.org/10.1021/cb400007k | ACS Chem. Biol. 2013, 8, 1063−1073

Table 2. Data Collection and Refinement Statistics; Values in Parentheses Correspond to Highest Resolution Shell

data set	Apo	CoA1	CoA2
wavelength (Å)	0.9393	0.8726	0.9393
space group	*C*2	*C*2	*C*2
unit cell *a*, *b*, *c* (Å)	249.5, 134.3, 118.4	248.2, 136.0, 118.2	248.3, 135.3, 118.6
β (deg)	110.7	110.4	110.6
resolution range (Å)	50−2.3 (2.42−2.3)	51.07−2.63 (2.77−2.63)	49.35−2.5(2.64−2.5)
R_{merge} (%)	11.6(55.3)	13.7 (70.4)	11.8(56.3)
R_{meas} (%)	13.3(63.5)	15.7 (80.6)	13.6(64.9)
$\langle I\rangle/\sigma\langle I\rangle$	10 (2.5)	8.5 (2.1)	9.1(2.5)
completeness (%)	99.9(100)	99.8 (99.0)	99.8(98.9)
multiplicity	4.1 (4.2)	4.3 (4.2)	4.1 (4.1)
Wilson B (Å^2)	33.8	50.7	41.9
no. of reflections	153278	103601	119944
no. of atoms			
protein	16818	16803	16861
ligand atoms/ions	204	328	418
waters	1026	779	837
av *B* factor (Å^2)			
protein atoms	32.3	38.8	37.5
ligand atoms/ions	50.7	66.3	56.2
waters	30.5	31.3	31.3
R_{work}/R_{free} (%)	19.5/22.4	18.6/23.0	18.1/22.1
rms bond (Å)	0.0052	0.0054	0.0065
rms angle (deg)	0.9848	1.0581	1.1780
rms chiral (Å^3)	0.0671	0.0718	0.0788
Ramachandran plot (%)			
favored	97.4	97.5	97.5
allowed	99.8	99.9	99.9
outliers	0.2	0.1	0.1
PDB entry	4B3H	4B3I	4B3J

open compared to subunit B. The most protruding region of the open HAD-specificity loop (residues Ala574-Gly575-Gly576) has moved by approximately 10 Å. This loop region, which has high *B*-factors, is a unique insertion in mtTFE (Supplementary Figure S1). In the closed conformation, the helices DH3 and DH4 move closer to helix DH1, near the HAD catalytic site, as defined by the catalytic His462-Glu474 diad. Two glycerol molecules are bound in the more open HAD catalytic site (subunit A). This binding pocket is narrower in subunit B (closed form), accommodating only one glycerol molecule. Glycerol has been used during the purification protocol and has apparently remained bound during the purification and crystallization steps.

Structure of the mtTFE-β Chain. The mtTFE-β subunit adopts the classical thiolase fold, being assembled into a thiolase dimer. The structures of the two mtTFE-β chains are identical. Each mtTFE-β chain consists of two topologically similar domains, namely, N-domain and C-domain made of a five-stranded β-sheet sandwiched between two helices on the outside (bulk solvent) and two buried helices on the inside and a third domain, referred to as the loop domain (Figure 2A,C). The loop domain is a long insertion of approximately 120 residues in the N-domain. The loop domain circles around the active site and provides important interactions with the CoA ligand. Continuous electron density is seen for both of the thiolase subunits from residues 2 to 403 with a break in the loop region 224−228, just before helix LA5 of the loop domain. This disordered part of the loop domain is near the CoA binding site.

Liganded Structures. Two data sets, namely, CoA1 and CoA2, were collected from two crystals of mtTFE grown in the presence of 2 mM CoA. The CoA1 data set is from a fresh crystal, whereas the CoA2 data set has been obtained from a crystal of the same drop, but harvested 1 month later. In the CoA1 structure, the ligand is bound in the two hydratase active sites with full occupancy. Its mode of binding confirms the importance of Glu119 and Glu141 for the catalysis.[14] In each of these liganded active sites a hydroxyl group of a glycerol is hydrogen-bonded to the catalytic water, which in turn is hydrogen-bonded to the side chain carboxylate atoms of the catalytic Glu119 and Glu141 (Figure 3A,B). In CoA2, the ligand is additionally bound to the two thiolase active sites. Although the ligand density is weaker in all of the active sites and is built with only 0.5 occupancy, this structure identifies the binding site of CoA in the thiolase subunit (Figure 3C). Overall, the CoA1 and CoA2 structures superpose very well with the apo structure. The only disordered region of the thiolase loop domain in the apo structure, just before helix LA5, is ordered in the CoA2 structure.

In the CoA1 and CoA2 structures, there is no ligand bound in the HAD active site (except for the glycerol molecules). The structures of the HAD-specificity loops are similar in the apo, CoA1, and CoA2 structures: open in subunit A and closed in subunit B. The CoA1 and CoA2 structures provide important structural information on the geometry of the active site substrate binding pocket of the hydratase and thiolase domains. The oxyanion hole of the hydratase active site for binding the thioester oxygen is preserved and shaped by N(Gly68) and N(Gly116) (Figure 3A,B). In the thiolase active site the two

dx.doi.org/10.1021/cb400007k | *ACS Chem. Biol.* 2013, 8, 1063−1073

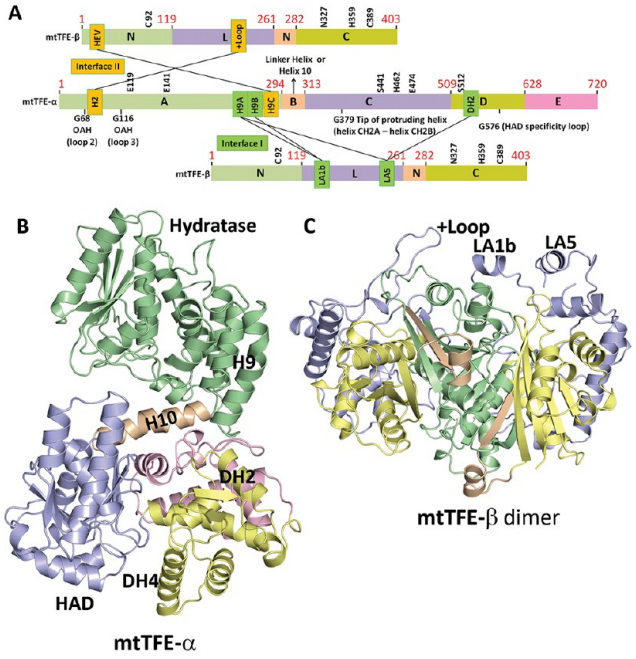

Figure 2. Domain organization and tertiary structure of the mtTFE-α and mtTFE-β subunits. (A) Color-coded and annotated schematic figure of the domains of mtTFE-α (in the middle) and mtTFE-β (above and below). The important residues are mentioned at their approximate positions. The important regions of interface between the α and β subunits are highlighted by green blocks for interface I (major interface) and yellow blocks for interface II (minor interface). The naming conventions are as in Supplementary Figures S1 and S2. (B) Tertiary structure of mtTFE-α subunit with the domains represented in same colors as in panel A. The main interface regions and linker helix (H10) are labeled. Also labeled is helix DH4, which adopts different conformations in the two α chains. Domains A and B together form the hydratase fold. Domains C, D, and E together form the HAD (dehydrogenase) fold. (C) Tertiary structure of mtTFE-β dimer with the domains as in panel A. The main interacting regions of mtTFE-β dimer with mtTFE-α, namely, LA1b, LA5 (subunit 1), and cationic loop (+Loop) (subunit-2) are labeled.

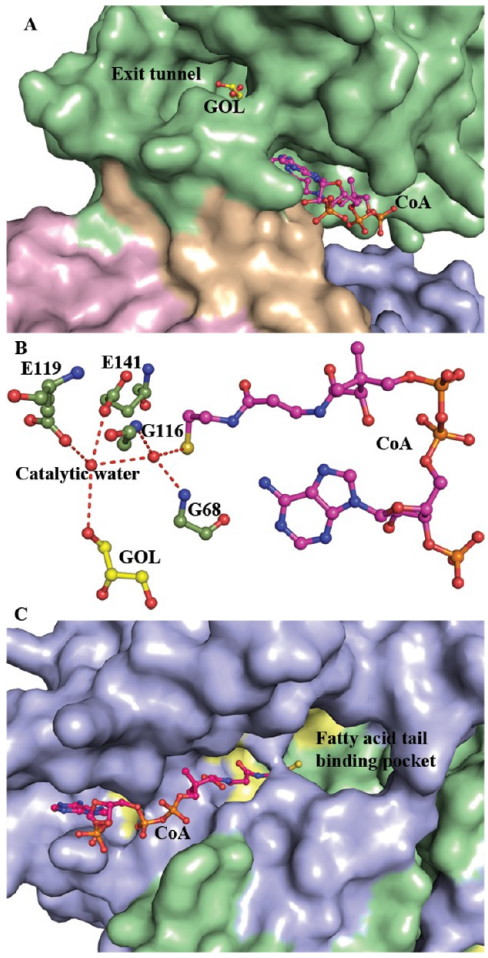

Figure 3. Liganded active sites of the hydratase domain of mtTFE-α and of mtTFE-β (thiolase). (A) The solvent exposed active site region of mtTFE-α hydratase domain with the CoA bound (ball and stick model in magenta) as in CoA1 structure. A glycerol molecule (GOL) bound at the exit path is shown in yellow ball and stick model. The mtTFE-α structure is shown in surface representation with the same color coding as in Figure 2. (B) A closer look at the hydratase active site. The glycerol at the exit path is hydrogen-bonded to the two catalytic glutamates (Glu119 and Glu141) via the catalytic water. The oxyanion hole is formed by the two glycines Gly68 and Gly116. The water molecule bound in this oxyanion hole is also shown. This water molecule mimics the mode of binding of the thioester oxygen of the fatty acyl-CoA. (C) The active site region of the mtTFE-β thiolase subunit with the CoA bound (ball and stick model in magenta) as in the CoA2 structure. The domains are colored as in Figure 2. The putative fatty acid tail binding pocket is highlighted.

oxyanion holes[26] are preserved as well, including the catalytic water between ND2(Asn327) and SG(Cys389). However, the trail of water molecules hydrogen-bonded to this catalytic water[26] is absent, because in the mtTFE structure larger hydrophobic side chains, like Leu326, clash with the waters of this water trail of the bacterial thiolase. Each of the four typical thiolase sequence fingerprints, identifying the four catalytic loops and the four catalytic residues,[27] Cys92, Asn327, His359, and Cys389, are preserved in mtTFE-β (Supplementary Figure S2).

Structural Comparisons. The hydratase catalytic site of mtTFE is well conserved when compared to pfTFE and the monofunctional enoyl-CoA hydratases.[28] The glycerol molecule that is hydrogen-bonded to the catalytic water in the mtTFE hydratase active site identifies a putative exit tunnel near loop-2 for binding of an extended fatty acid tail (Figure 3A), different in unliganded pfTFE and monofuntional enzymes. A possible position for the binding of an extended fatty acid tail in the HAD active site can be inferred by comparing mtTFE with the ternary complex structure of monofunctional mitochondrial HAD complexed with NAD^+ and acetoacetyl-CoA. From this it is predicted that the fatty acid tail binds in the empty pocket between DH1 and DH4.[29] In mtTFE-α (subunit A), the helix DH4 has moved away from DH1 generating more space, and this space is occupied by an extra glycerol molecule. This space is not present in pfTFE. Also, in mtTFE there is a serine (Ser512) in the place of a highly conserved asparagine lining this pocket (at the N-terminus of helix DH1). In addition, this pocket is lined by Gly516 (corresponding to Phe505 in pfTFE, Supplementary Figure S2) and the hydrophobic side chains of Met560 and Ile563 (helix DH4). These structural features should play a crucial role in influencing the substrate specificity of mtTFE, probably accommodating more bulky fatty acid chains in mtTFE.

The overall fold of the mtTFE and pfTFE thiolase is similar. The mode of binding of the CoA moiety to mtTFE and pfTFE is the same, except for the outward placement of the reactive β-

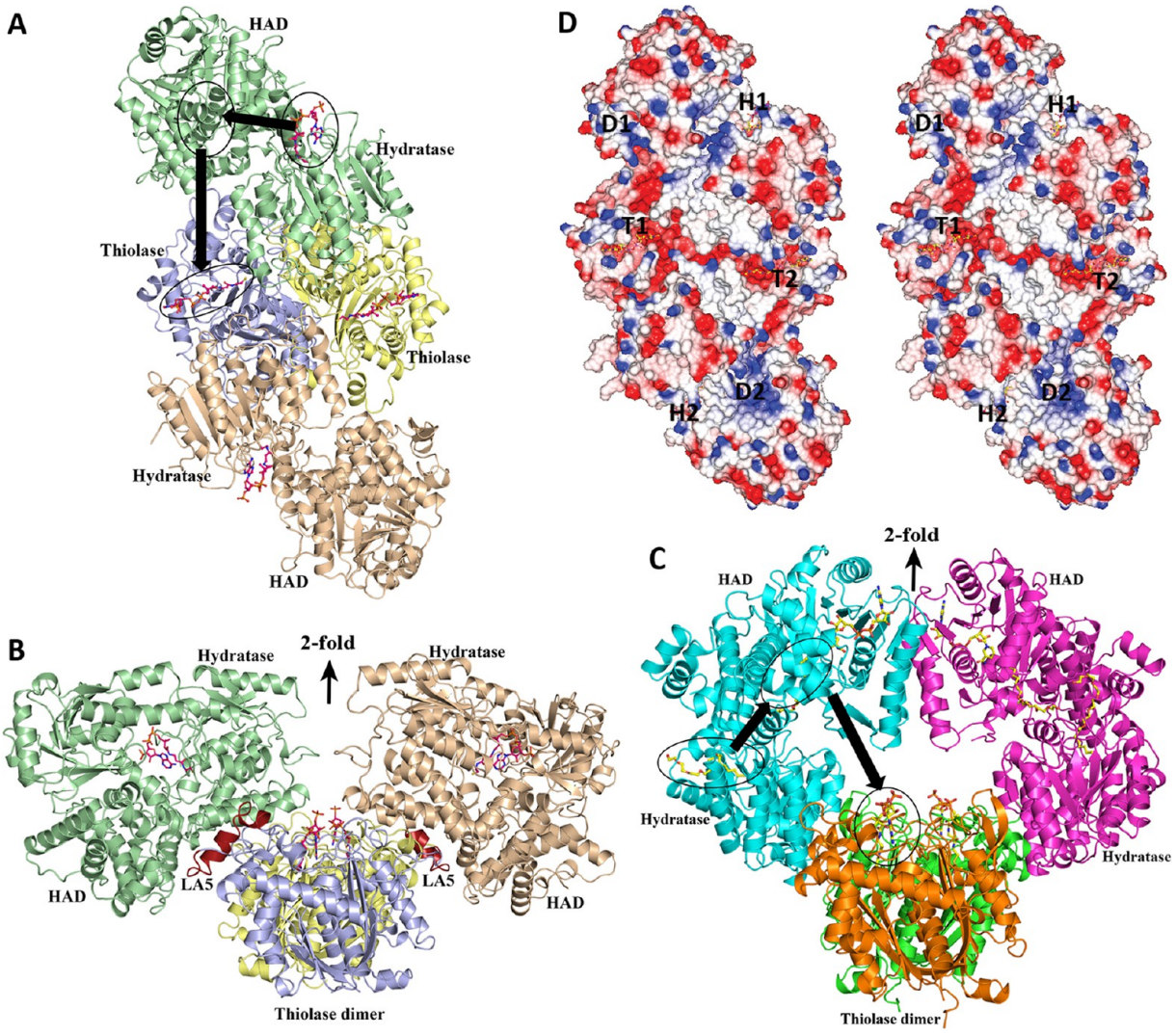

Figure 4. Quaternary assembly of mtTFE and pfTFE. (A) Top view of the mtTFE assembly. The β (thiolase) dimer is at the center in blue and yellow cartoon. The two α subunits are shown in green and brown. The CoA molecules bound at the hydratase and the thiolase active sites are shown in magenta ball and stick model. The approximate regions of the active sites are highlighted in circles, and the direction of transfer of substrates from one active site to the other is shown with arrows. (B) Side view of the mtTFE assembly highlighting the non-crystallographic 2-fold symmetry (running vertically in the center) between the two α-subunits. This orientation also clearly shows that the two α-subunits do not interact with each other. Helix LA5 of each β chain is highlighted in red. (C) pfTFE assembly: the thiolase unit is in the same orientation as in panel B, highlighting the different mode of assembly of the two α-subunits (cyan and magenta) over the two β-subunits (green and orange). The approximate active site regions and the direction of transfer of substrates are highlighted with circles and arrows. The three domains are named in all panels. (D) Stereo diagram of electrostatic surface potential of mtTFE calculated using CCP4MG[47] in the same view as in panel A. Surface areas of positive potential are colored blue, and surface areas of negative potential are colored red. The hydratase, dehydrogenase (HAD), and thiolase active sites, labeled as H1, D1, T1 and H2, D2, T2, are connected via the two proposed substrate channeling paths, respectively.

mercaptoethylamine part in the mtTFE active site. Nevertheless, the geometry of the thiolase catalytic site[26] is preserved in the mtTFE active site. A putative binding pocket for the fatty acid tail can be identified by noting structural similarities of the LA1b region of the mtTFE-β subunit with the yeast peroxisomal thiolase structure, which is also a degradative dimeric thiolase.[30] The binding site for the fatty acid tail is shaped by the residues corresponding to the region between Asp130 and Gln149 of mtTFE, at the beginning of the loop domain (Supplementary Figure S2). This putative fatty acid tail binding pocket in mtTFE is larger and more solvent exposed (Figure 3C) than in pfTFE, due to the presence of small side chains (Gly67 instead of Trp70 and Leu361 instead of Phe349) in mtTFE and therefore could accommodate bulky fatty acid chains. These residues are located at the rim of this binding pocket. Also the main chain trace just before helix LA2, Pro148-Gln149-Ser150 instead of Gly149-Met150-Met151, generates a more solvent accessible fatty acid tail binding pocket in mtTFE, not present in pfTFE. This extra space is to some extent being filled by the β-mercaptoethylamine part of CoA in the CoA2 complex.

The key structural differences between the mtTFE and pfTFE thiolase subunits are in the thiolase loop domain. This concerns the beginning of the loop domain, near helix LA1b, the structures of the cationic loop, and the properties of helix LA5 of mtTFE (Figure 2C). Helix LA5 is at the end of the loop domain and is a novel structural feature of the mtTFE structure, not seen in any of the previously characterized thiolase structures. The significance of the helix LA5 in the assembly is discussed in the following sections.

dx.doi.org/10.1021/cb400007k | ACS Chem. Biol. 2013, 8, 1063−1073

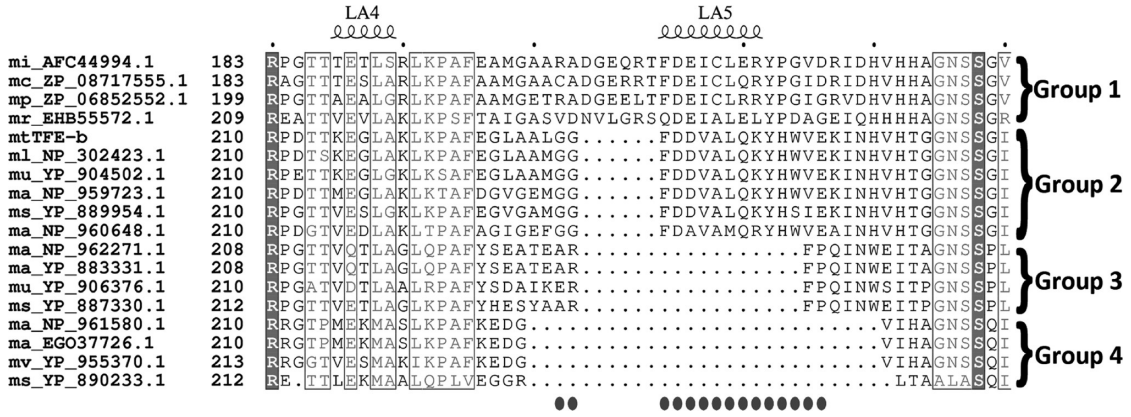

Figure 5. Part of the multiple sequence alignment of a subset of mycobacterial thiolase sequences. Each sequence is identified by a unique sequence identifier, shown on the left. The secondary structure elements correspond to mtTFE-β. The four sequence groups are named on the right.

Assembly of the mtTFE $\alpha_2\beta_2$-Complex. The mtTFE and pfTFE share a sequence identity of 33% and 40% for the α and the β chains, respectively. The tertiary structures of the individual subunits of mtTFE and pfTFE are quite similar with rmsd values of 2.3 and 1.2 Å for the superposition of corresponding Cα atoms of the α and β chains, respectively. Also, in both assemblies, the TFE-β (thiolase) dimer provides the scaffold on which the two TFE-α chains assemble. The two TFE-β dimers superpose well on each other, having a rmsd of 1.5 Å for the superposition of corresponding Cα atoms. However, the orientation of the two TFE-α chains with respect to the TFE-β dimer is totally different in mtTFE. Despite this, helix H9A of the α chain is involved in protein−protein interactions with the thiolase loop domain in both mtTFE and pfTFE. This results in a completely new quaternary structure for mtTFE (Figure 4A,B). The main reason for the alternative orientation of the α chain with respect to the β chain is due to the presence of an extra helix (helix LA5, residues 232−246) in the loop domain of mtTFE-β (Figure 2C, Figure 4B, Supplementary Figure S2). This helical insertion in mtTFE-β prevents the pfTFE mode of assembly, as it would clash completely with the H9A helix of the α chain. Also, in the mtTFE assembly the two mtTFE-α chains of the $\alpha_2\beta_2$-complex do not interact with each other as in pfTFE (Figure 4B). Nevertheless, they are strictly related by the same 2-fold axis of the mtTFE-β dimer (Figure 4B,C). In pfTFE the HAD parts interact with each other via this 2-fold axis, whereas in pfTFE the HAD parts point away from this 2-fold axis. The closest contact between the two mtTFE-α chains is in the region Ser234-Ser235-Pro236, being 10 Å away from each other. This region is a unique insertion in the mtTFE-α sequence, just before helix H9A (Supplementary Figure S1). In the pfTFE assembly only the hydratase domain interacts with the thiolase dimer, whereas in the mtTFE assembly both the hydratase domain as well as the HAD-part interact with the thiolase dimer. The mtTFE-α chain interacts with both subunits of the mtTFE-β dimer. These interactions are dominated by two helices in the thiolase loop domain (LA1b and LA5), which interact with helices H9A, H9B (hydratase part) and DH2, DH6 (dehydrogenase part) at interface I (1100 Å^2; Figure 2A). At this interface helix H9A is wedged between helices LA1b and LA5. These interactions tightly fix the A, D and E domains of the mtTFE-α chain and the mtTFE-β dimer together. This interaction is complemented by a weaker interaction (interface II; 500 Å^2) between the LA1b and the cationic loop of thiolase with helices H9C and H2 of the hydratase domain. The differences in assembly are also reflected in differences in the properties of the TFE-α chain in the absence of the TFE-β subunit. The pfTFE-α chain is a dimer,[31] whereas the mtTFE-α chain is a monomer. The pfTFE assembly forms a ring-like structure with each of the active sites facing a central reaction chamber whereas the active sites are more bulk solvent exposed in mtTFE (Figure 4C). The tight interactions between the mtTFE-α and β chains very much suggest that the heterotetramer present in the asymmetric unit represents the active tetramer in solution.

From sequence alignments it is also found that the *Mycobacterium avium* thiolase FadA1, whose crystal structure (PDB id: 3SVK) has been deposited recently, has the same unique sequence features as mtTFE-β. This gene is also part of an operon encoding an α chain and a β chain. This sequence includes the LA5-helix as well as the LA1b sequence. Interestingly, in this structure the thiolase dimer is present as seen in the mtTFE thiolase, but the LA5 and LA1b regions are mostly disordered, suggesting that the complex formation with the α chain is required for adopting the ordered fold, as seen in this mtTFE structure.

Substrate Channeling. The intermediates of the β-oxidation pathway are the highly polar and negatively charged CoA derivative molecules. The mechanism of substrate channeling for highly polar negatively charged substrate molecules is poorly understood. A key feature of the pfTFE complex is the flexibility of the assembly.[32] In one form (form I, PDB id: 1WDK), the pfTFE tetramer is symmetric and the 2-fold axes of α2 and β2 coincide (Figure 4C). In another, asymmetric, form (form IV, PDB id: 1WDL) the HAD part of the α chain is shifted by about 10 Å closer to the thiolase dimer. This flexibility and the characteristic ring-like structure has been the basis of the proposed substrate channeling path of pfTFE. Interestingly, in mtTFE the channeling pathway is different since in the mtTFE assembly the location of the active sites of the α chain with respect to the β chain is totally dissimilar (Figure 4A,B). In addition, the mtTFE assembly appears to be more rigid; for example, ligand (CoA) binding to the mtTFE complex structure does not induce structural changes. Also, as stated above, in pfTFE only the hydratase domain interacts with the thiolase dimer, whereas in mtTFE all domains of the α chain, except the C-domain, interact with the thiolase dimer. The surface features of the mtTFE-complex, shown in Figure 4D, identify a groove between the three active sites, which is

dx.doi.org/10.1021/cb400007k | *ACS Chem. Biol.* 2013, 8, 1063−1073

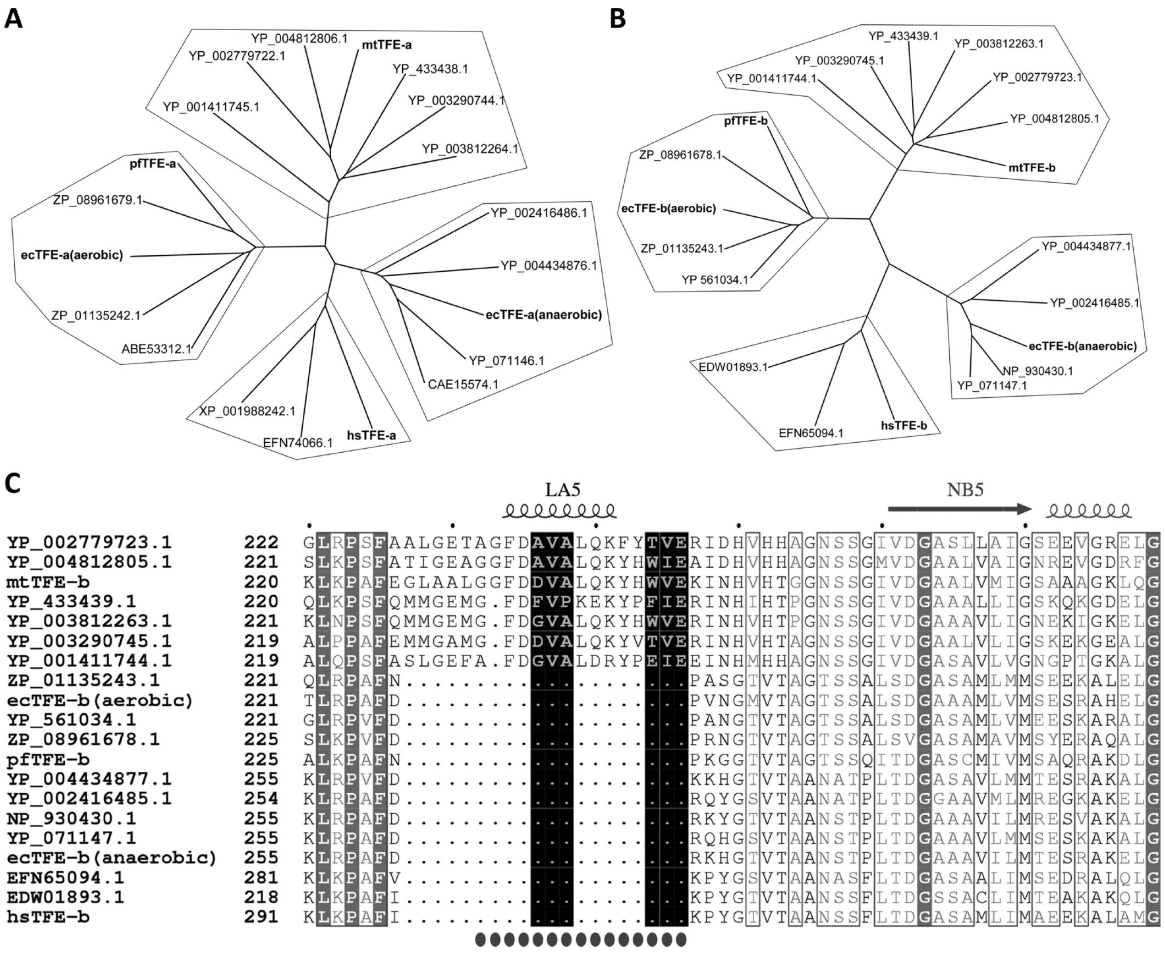

Figure 6. Clustering of TFE sequences into four subfamilies. (A) Phylogenetic tree of TFE-α sequences from various organisms. The query sequences that were used to retrieve other sequences from the sequence database are in bold. Other sequences are represented by their unique identifiers. (B) Phylogenetic tree of the TFE-β sequences corresponding to those in top left panel. (C) Part of the multiple sequence alignment of the TFE-β sequences that were used to construct the phylogenetic tree. The unique sequence insertion region (including helix LA5) is highlighted by dots at the bottom of the sequence alignment. The secondary structure elements corresponding to mtTFE-β are shown at the top of the sequence alignment. The sequences are named as in panel B.

devoid of negatively charged patches. Along this surface path in the mtTFE complex the active sites are chronologically placed, such that the distance between the hydratase active site (at the outer rim of the complex) and the HAD active site is 39 Å and the distance between the HAD active site and the thiolase active site (at the center of the complex) is 55 Å. The substrate could crawl from one active site to the other by anchoring through this path without diffusing into the bulk solvent (Figure 4D).

TFE-Like Thiolase Sequences in Mycobacterial Species. Inspection of the Mtb genome shows that Mtb has only one TFE-α chain, but several thiolase chains. One of these thiolase sequences, the mtFadA2 gene, is more closely related to the human TFE-β (35% identity) than to mtTFE-β (27% identity). The mtFadA2 gene is not part of any operon suitable for coding the β chain with an adjacent α chain. This sequence analysis also shows that the unique LA5 region of mtTFE-β is absent in the mtFadA2 gene sequence (Supplementary Figure S2). The mtFadA2 gene was cloned in the place of mtTFE-β and was coexpressed with mtTFE-α to check if these two proteins form a complex similar to pfTFE. The mtFadA2 gene was expressed, and the protein was in the soluble fraction but did not co-purify with the his-tagged mtTFE-α by Ni-NTA affinity chromatography. Instead, it was in the unbound fraction (Supplementary Figure S3). The identity of the protein was confirmed from the SDS-PAGE band by MALDI mass spectrometry. These experiments show that mtFadA2 does not form a complex with mtTFE-α.

A search against mycobacterial genomes using the mtTFE-β as the query sequence resulted in many thiolase sequences. These sequences cluster into four categories with respect to the length of the unique LA5 insertion region in mtTFE-β (Figure 5) (Groups 1−4). Sequences belonging to Group 1 have a slightly longer insertion than the mtTFE-β, and not much information about these sequences is available in the sequence database currently. The Group 2 sequences have a similar insertion as in mtTFE-β. Notably, all Group 2 sequences have one immediately adjacent gene corresponding to a TFE-α chain in their genome. Sequences of Group 3 have a shorter insertion, and sequences of Group 4 do not have any sequence insertion in this region. It is interesting to point out that the genes corresponding to Group 3 were isolated thiolase-like gene sequences, whereas genes corresponding to Group 4 are located near genes corresponding to proteins such as acylCoA dehydrogenases and enoylCoA hydratases/isomerases, being also involved in fatty acid metabolism in their respective

dx.doi.org/10.1021/cb400007k | ACS Chem. Biol. 2013, 8, 1063−1073

genomes. In general, the database annotation information for most of these sequences is incomplete. From our analysis we can clearly say that all of the sequences falling in Group 2 are indeed TFE-thiolases, whereas thiolase sequences belonging to Groups 1, 3, and 4 can be referred as TFE-like thiolases whose physiological functions are not currently known. Further structural enzymological studies of these enzymes are required to understand better their role in the poorly characterized lipid metabolism of mycobacterial species.

Phylogenetic Tree Analysis of the TFEs. TFEs are poorly characterized, in general. Our studies show that there are at least two ways in which the two chains of TFE can assemble. We retrieved several TFE-α sequences from the nonredundant (nr) database using BLAST searches. TFE-α sequences from human, Mtb, *P. fragi*, and *E. coli* were used as the query sequence. Genus of the query sequences were excluded from the respective search. *E. coli* has two TFE complexes: the well characterized aerobic TFE[33] and the more recently discovered anaerobic TFE.[34] All of the retrieved sequences nicely group into four TFE-α subfamilies (Figure 6A). *P. fragi* and *E. coli* aerobic TFE-α's are in one subfamily (ec-arTFE subfamily). TFEs from higher eukaryotes including human TFE form another subfamily (hsTFE subfamily). *E. coli* anaerobic TFE and related sequences formed a third subfamily (ec-anTFE subfamily), which is more closely related to the hsTFE subfamily than to the ec-arTFE subfamily. Finally, mtTFE-α with a few other bacterial sequences formed a separate, fourth subfamily (mtTFE subfamily). Interestingly, when a phylogenetic tree was independently constructed for the corresponding TFE-β sequences, a very similar distribution was observed (Figure 6B). This shows that the TFE-α and -β sequences have coevolved.

From our structural studies it is clearly demonstrated that the two different TFE assemblies arise mainly due to the presence of the unique insertion (LA5) in mtTFE-β. All other sequences that grouped into this subfamily also have this sequence insertion (Figure 6C). The corresponding TFEs should then have a similar assembly as in mtTFE. Similarly, TFEs in the ec-arTFE subfamily whose TFE-β sequences do not have this sequence insertion should assemble as in pfTFE. Some of the mycobacterial species such as *M. aviam, M. van*, and *M. mcs* have two TFE complexes in their genomes. All of these TFE-β sequences also have this unique insertion and belong to the mtTFE family, unlike in *E. coli* where the additional TFE (anaerobic) forms a separate subfamily. Furthermore, although the hsTFE-thiolases do not have the unique LA5 insertion region as in mtTFE, these sequences have other insertions and deletions, unique to the hsTFE subfamily (Supplementary Figure S1, Supplementary Figure S2). It is also interesting to note that the human TFE is known to be associated to membranes and able to form hetero-octamers. Therefore, a more extensive characterization is required to know if the hsTFE subfamily forms tetramers similar to that of pfTFE or yet another new assembly.

Concluding Remarks. These studies for the first time characterize structural and kinetic properties of mtTFE. The structure of this mtTFE complex highlights the versatile mode by which these multifunctional enzymes can generate different assemblies. The biochemical studies of mtTFE show that the complex is more active than the individual α chain using *trans*-2-decenoyl CoA as the substrate. From structural comparisons it appears that each of the three acyl binding pockets of the mtTFE active sites are larger than for pfTFE, suggesting a different substrate specificity, such that CoA esters of more bulky fatty acid tails can possibly be degraded. The different assembly correlates with the presence of a unique helical insertion, LA5 (residues 232−246) present in the mycobacterial TFE-β sequences. In mtTFE, each of the domains are more rigidly fixed with respect to each other than in pfTFE except for the nucleotide binding domain, domain C, of the HAD part. Also the active sites of the α chains are completely differently positioned with respect to the β dimer. The spatial arrangement of the mtTFE active sites allows for a path facing bulk solvent for substrate transfer between these three active sites. Further studies are required to establish if and how the substrates are channeled through this path. In any case, for the above-mentioned reasons, the substrate channeling path as proposed for the pfTFE does not apply to the mtTFE. A sequence analysis shows that there are at least four TFE subfamilies. The current structure and sequence analysis has significantly extended our knowledge and opened new opportunities to study the intriguing structural enzymological properties of this important but poorly characterized family of TFEs.

METHODS

Cloning, Expression, and Purification. Synthetic genes were obtained for mtFadA (mtTFE-β), mtFadB (mtTFE-α), and mtFadA2 from Mr.Gene (now: Life technologies). The gene sequences were optimized for better expression in *E. coli*. mtTFE-α and mtTFE-β were cloned into pACYC- and pET-Duet (Novagen) at multiple cloning sites MCSI and MCSII, respectively, resulting in a clone that could express mtTFE-α with a hexa-histidine tag at the N-terminus. The mtFadA2 gene was cloned into MCSII of pACYC-Duet, which contained mtTFE-α at MCSI. The double clone having mtTFE-β and mtTFE-α in pET-Duet at MCSII and MCSI (mtTFE) and the double clone having mtFadA2 and mtTFE-α in pACYC-Duet at MCSII and MCSI (mtFadA2B) were used for further expression and purification.

The mtTFE and mtFadA2B were expressed in BL21 (DE3) strain of *E. coli*. The cells were grown in M9ZB media at 37 °C. When the cells were grown to an OD (at 600 nm) of 0.6, the growth temperature was reduced to 25 °C, and the expression of the protein was induced by adding IPTG to a final concentration of 0.2 mM. The cells were harvested after 5 h and resuspended in the lysis buffer (20 mM Tris, 500 mM NaCl, 10% glycerol, 0.1% Triton-X, and 5 mM imidazole pH 7.8). The cells were lyzed by sonication, and the expression was checked in 12% SDS-PAGE. mtTFE-α and mtTFE-β were coexpressed.

The enzyme was purified by Ni-NTA affinity chromatography followed by anion exchange chromatography using a 6 mL Resource-Q column. This resulted in the separation of mtTFE complex and the uncomplexed mtTFE-α. The complex as well as the α chain was further purified by size exclusion chromatography (HiLoad 16/60 Superdex 200 column (GE Healthcare) pre-equilibrated with 20 mM HEPES buffer pH 7.2 containing 120 mM KCl, 1 mM EDTA, and 1 mM sodium azide). The molecular mass and the oligomeric state of the eluted peaks were determined by SLS detector (miniDawn Treos, Wyatt Technologies) and refractive index (RI) detector (RI-101, Shodex).

Enzyme Assays. *trans*-2-Decenoyl CoA was used as the substrate for all the activity measurements, always at 25 °C. The *trans*-2-decenoyl CoA was synthesized as described previously.[35] The enoyl CoA hydratase (ECH) activity of mtTFE and mtTFE-α subunit was measured at 263 nm as the disappearance of the C−C double bond of the substrate. The reaction mixture (total volume 0.5 mL) contained 50 mM Tris (pH 8.5), 50 mM KCl, 50 μg mL^{-1} BSA, and 60 μM substrate. The reaction was initiated by the addition of 5 ng of mtTFE or 10 ng of mtTFE-α to the reaction mixture. The K_m and k_{cat} values were determined by repeating the assay at various substrate concentrations from 3 to 120 μM. Absorption coefficient of 6700

M^{-1} cm^{-1} for *trans*-2-decenoyl CoA was used for the calculation of the catalytic rates.[36]

The 3-hydroxyacyl CoA dehydrogenase (HAD) activity was monitored by the formation of NADH at 340 nm (absorption coefficient 6220 M^{-1} cm^{-1}). The reaction mixture contained 50 mM Tris (pH 8.5), 50 mM KCl, 50 μg mL^{-1} BSA, 1 mM CoA, 1 mM NAD^+, and 60 μM substrate. The reaction was initiated by the addition of 100 ng of mtTFE or 200 ng of mtTFE-α. For determining the K_m and k_{cat} values the assay was repeated at various substrate concentrations from 0.6 to 60 μM. The K_m and k_{cat} values reported in Table 1 are the average of at least three independent measurements, and the reported errors are the standard deviations of these measurements.

To measure the thiolase activity of mtTFE, the substrate *trans*-2-decenoyl CoA was converted to 3-ketodecanoyl CoA by the ECH and HAD reactions by incubating the reaction mixture for 15 min at RT. The reaction mixture contained 50 mM Tris (pH 8.5), 50 mM KCl, 50 μg/mL^{-1} BSA, 0.5 mM NAD^+, 5 mM $MgCl_2$, and 60 μM substrate. The 3-ketodecanoyl CoA forms a coordination complex with Mg^{2+}, which absorbs at 303 nm. The thiolase reaction was then initiated by the addition of 0.5 mM CoA resulting in the disappearance of the 3-ketodecanoyl CoA and thus the reduction in the absorbance at 303 nm. The catalytic rate using such an assay has been calculated with the absorption coefficient of 13900 M^{-1} cm^{-1} for the Mg^{2+}-keto complex.[37] The results are summarized in Table 1.

Crystallization and Data Collection. The mtTFE complex crystallized in the presence of 2 M ammonium sulfate in 100 mM Tris buffer at pH 8.5 by sitting drop vapor diffusion method at RT. mtTFE was crystallized as apo protein and cocrystallized with 2 mM CoA. The crystallization drops were made by mixing 1 μL of protein solution at a concentration of 6 mg $mL^{-1}$with 1 μL of well solution. The crystals were very sensitive on exposure to air and to cryoprotectants like glycerol, ethylene glycol, MPD, and PEGs. Therefore, crystals were frozen directly in liquid nitrogen without using any cryoprotectant. Three data sets were collected at the ID23-2 and ID14-4 beamlines at the ESRF. The data were processed and scaled using the programs iMOSFLM,[38] SCALA,[39] and XDS.[40] The data collection and quality statistics are summarized in Table 2.

Structure Determination and Analysis. TFE complex from *Pseudomonas fragi* (pfTFE; PDB id: 1WDK)[15] was used as the molecular replacement model to solve the structure of mtTFE using the program PHASER.[41] A valid solution could only be obtained when the N- and C-terminal domains of the α chain as well as the separate β chain were given as separate polypeptide units. The asymmetric unit in the crystal structure consisted of two mtTFE-α and two mtTFE-β subunits. The structures were further refined by REFMAC5[42] of CCP4,[43] and the model was built using COOT[44] in iterative cycles. The progress of the refinement was cross-validated by using a 5% set of R_{free} reflections. Water and ligand molecules were added during the last few cycles of refinement and model building. The refinement and model quality statistics are summarized in Table 2. Validation tools from MOLPROBITY were used for validating the refined structures.[45] The interfaces were analyzed using the program PISA.[46] The calculations for the electrostatic surface were done with CCP4MG.[47] The figures were drawn using the program PyMol.[48] The secondary structure assignments were calculated using the program DSSP.[49]

Phylogenetic Tree Construction. TFE-α sequences from human, Mtb, Pf, and *E. coli* (both aerobic and anaerobic) were used as query sequences for BLAST[50] runs against the nr database excluding the genomes from the same genus. The top 200 sequences were retrieved from each BLAST run and combined. These sequences were then clustered with a sequence identity cut-off of 60% using the web-based CDHIT[51] suit. One representative sequence from each cluster was taken for further sequence alignment. The multiple sequence alignments were done with the web-based CLUSTALW2 program,[52] and the guide tree obtained was used to construct a phylogenetic tree using the program TreeView.[53] Similarly, a phylogenetic tree was constructed for the corresponding TFE-β sequences. The sequence and secondary structure figures were drawn using the web-based program ESPript.[54]

■ ASSOCIATED CONTENT

Supporting Information

Additional figures. This material is available free of charge via the Internet at http://pubs.acs.org.

Accession Codes

The atomic coordinates and structure factors have been deposited in the Protein Data Bank. The PDB id codes are 4B3H, 4B3I, and 4B3J as listed in Table 2.

■ AUTHOR INFORMATION

Corresponding Author

*E-mail: rik.wierenga@oulu.fi.

Notes

The authors declare no competing financial interest.

■ ACKNOWLEDGMENTS

The authors wish to thank W. Schmitz for providing *trans*-2-decenoyl CoA. The authors acknowledge ESRF, Grenoble for expert support of the X-ray crystallographic data collection. This work was supported by the Academy of Finland grant 24300431.

■ ABBREVIATIONS

Mtb, *Mycobacterium tuberculosis*; TFE, trifunctional enzyme; mtTFE, Mtb TFE; pfTFE, *Pseudomonas fragi* TFE; mtTFE-α, the α chain of mtTFE; mtTFE-β, the β chain of mtTFE; MFE1, the monomeric multifunctional enzyme, type-1; HAD, L-3-hydroxyacyl-CoA dehydrogenase; SLS, static light scattering

■ REFERENCES

(1) Young, D. B. (1998) Blueprint for the white plague. *Nature 393*, 515−516.

(2) Willyard, C. (2012) Race heats up for first-to-market drugs for resistant tuberculosis. *Nat. Med. 18*, 1157−1157.

(3) Munoz-Elias, E. J., and McKinney, J. D. (2005) *Mycobacterium tuberculosis* isocitrate lyases 1 and 2 are jointly required for in vivo growth and virulence. *Nat. Med. 11*, 638−644.

(4) Thomas, S. T., VanderVen, B. C., Sherman, D. R., Russell, D. G., and Sampson, N. S. (2011) Pathway profiling in *Mycobacterium tuberculosis*: Elucidation of cholesterol-derived catabolite and enzymes that catalyze its metabolism. *J. Biol. Chem. 286*, 43668−43678.

(5) Chang, J. C., Miner, M. D., Pandey, A. K., Gill, W. P., Harik, N. S., Sassetti, C. M., and Sherman, D. R. (2009) Igr genes and *Mycobacterium tuberculosis* cholesterol metabolism. *J. Bacteriol. 191*, 5232−5239.

(6) Cole, S. T., Brosch, R., Parkhill, J., Garnier, T., Churcher, C., Harris, D., Gordon, S. V., Eiglmeier, K., Gas, S., Barry, C. E., 3rd, Tekaia, F., Badcock, K., Basham, D., Brown, D., Chillingworth, T., Connor, R., Davies, R., Devlin, K., Feltwell, T., Gentles, S., Hamlin, N., Holroyd, S., Hornsby, T., Jagels, K., Krogh, A., McLean, J., Moule, S., Murphy, L., Oliver, K., Osborne, J., Quail, M. A., Rajandream, M. A., Rogers, J., Rutter, S., Seeger, K., Skelton, J., Squares, R., Squares, S., Sulston, J. E., Taylor, K., Whitehead, S., and Barrell, B. G. (1998) Deciphering the biology of *Mycobacterium tuberculosis* from the complete genome sequence. *Nature 393*, 537−544.

(7) Camus, J. C., Pryor, M. J., Medigue, C., and Cole, S. T. (2002) Re-annotation of the genome sequence of *Mycobacterium tuberculosis* H37Rv. *Microbiology 148*, 2967−2973.

(8) Fould, B., Garlatti, V., Neumann, E., Fenel, D., Gaboriaud, C., and Arlaud, G. J. (2010) Structural and functional characterization of the recombinant human mitochondrial trifunctional protein. *Biochemistry 49*, 8608−8617.

(9) Dellomonaco, C., Clomburg, J. M., Miller, E. N., and Gonzalez, R. (2011) Engineered reversal of the beta-oxidation cycle for the synthesis of fuels and chemicals. *Nature 476*, 355−359.

(10) Zhang, H., Machutta, C. A., and Tonge, P. J. (2010) Fatty Acid Biosynthesis and Oxidation, in *Comprehensive Natural Products II: Chemistry and Biology* (Mander, L., and Liu, H., Eds.) 1st ed., pp 231−275, Elesvier, Oxford.
(11) Papai, I., Hamza, A., Pihko, P. M., and Wierenga, R. K. (2011) Stereoelectronic requirements for optimal hydrogen-bond-catalyzed enolization. *Chemistry 17*, 2859−2866.
(12) Bhaumik, P., Koski, M. K., Glumoff, T., Hiltunen, J. K., and Wierenga, R. K. (2005) Structural biology of the thioester-dependent degradation and synthesis of fatty acids. *Curr. Opin. Struct. Biol. 15*, 621−628.
(13) Liang, X., Le, W., Zhang, D., and Schulz, H. (2001) Impact of the intramitochondrial enzyme organization on fatty acid oxidation. *Biochem. Soc. Trans. 29*, 279−282.
(14) He, X. Y., and Yang, S. Y. (1997) Glutamate-119 of the large alpha-subunit is the catalytic base in the hydration of 2-trans-enoyl-coenzyme A catalyzed by the multienzyme complex of fatty acid oxidation from *Escherichia coli*. *Biochemistry 36*, 11044−11049.
(15) Ishikawa, M., Tsuchiya, D., Oyama, T., Tsunaka, Y., and Morikawa, K. (2004) Structural basis for channelling mechanism of a fatty acid beta-oxidation multienzyme complex. *EMBO J. 23*, 2745−2754.
(16) Imamura, S., Ueda, S., Mizugaki, M., and Kawaguchi, A. (1990) Purification of the multienzyme complex for fatty acid oxidation from *Pseudomonas fragi* and reconstitution of the fatty acid oxidation system. *J. Biochem. 107*, 184−189.
(17) Anderson, K. S. (1999) Fundamental mechanisms of substrate channeling. *Methods Enzymol. 308*, 111−145.
(18) Hyde, C. C., Ahmed, S. A., Padlan, E. A., Miles, E. W., and Davies, D. R. (1988) Three-dimensional structure of the tryptophan synthase alpha 2 beta 2 multienzyme complex from *Salmonella typhimurium*. *J. Biol. Chem. 263*, 17857−17871.
(19) Manjasetty, B. A., Powlowski, J., and Vrielink, A. (2003) Crystal structure of a bifunctional aldolase-dehydrogenase: Sequestering a reactive and volatile intermediate. *Proc. Natl. Acad. Sci. U.S.A. 100*, 6992−6997.
(20) Meek, T. D., Garvey, E. P., and Santi, D. V. (1985) Purification and characterization of the bifunctional thymidylate synthetase-dihydrofolate reductase from methotrexate-resistant *Leishmania tropica*. *Biochemistry 24*, 678−686.
(21) Eaton, S., Bartlett, K., and Pourfarzam, M. (1996) Mammalian mitochondrial beta-oxidation. *Biochem. J. 320* (Pt 2), 345−357.
(22) Yao, K. W., and Schulz, H. (1996) Intermediate channeling on the trifunctional beta-oxidation complex from pig heart mitochondria. *J. Biol. Chem. 271*, 17816−17820.
(23) Eaton, S., Bursby, T., Middleton, B., Pourfarzam, M., Mills, K., Johnson, A. W., and Bartlett, K. (2000) The mitochondrial trifunctional protein: Centre of a beta-oxidation metabolon? *Biochem. Soc. Trans. 28*, 177−182.
(24) Kasaragod, P., Venkatesan, R., Kiema, T. R., Hiltunen, J. K., and Wierenga, R. K. (2010) Crystal structure of liganded rat peroxisomal multifunctional enzyme type 1: A flexible molecule with two interconnected active sites. *J. Biol. Chem. 285*, 24089−24098.
(25) Arent, S., Christensen, C. E., Pye, V. E., Norgaard, A., and Henriksen, A. (2010) The multifunctional protein in peroxisomal beta-oxidation: Structure and substrate specificity of the arabidopsis thaliana protein MFP2. *J. Biol. Chem. 285*, 24066−24077.
(26) Merilainen, G., Poikela, V., Kursula, P., and Wierenga, R. K. (2009) The thiolase reaction mechanism: The importance of Asn316 and His348 for stabilizing the enolate intermediate of the claisen condensation. *Biochemistry 48*, 11011−11025.
(27) Haapalainen, A. M., Merilainen, G., and Wierenga, R. K. (2006) The thiolase superfamily: Condensing enzymes with diverse reaction specificities. *Trends Biochem. Sci. 31*, 64−71.
(28) Engel, C. K., Kiema, T. R., Hiltunen, J. K., and Wierenga, R. K. (1998) The crystal structure of enoyl-CoA hydratase complexed with octanoyl-CoA reveals the structural adaptations required for binding of a long chain fatty acid-CoA molecule. *J. Mol. Biol. 275*, 847−859.
(29) Barycki, J. J., O'Brien, L. K., Strauss, A. W., and Banaszak, L. J. (2000) Sequestration of the active site by interdomain shifting. crystallographic and spectroscopic evidence for distinct conformations of L-3-hydroxyacyl-CoA dehydrogenase. *J. Biol. Chem. 275*, 27186−27196.
(30) Mathieu, M., Modis, Y., Zeelen, J. P., Engel, C. K., Abagyan, R. A., Ahlberg, A., Rasmussen, B., Lamzin, V. S., Kunau, W. H., and Wierenga, R. K. (1997) The 1.8 A crystal structure of the dimeric peroxisomal 3-ketoacyl-CoA thiolase of *Saccharomyces cerevisiae*: Implications for substrate binding and reaction mechanism. *J. Mol. Biol. 273*, 714−728.
(31) Ishikawa, M., Mikami, Y., Usukura, J., Iwasaki, H., Shinagawa, H., and Morikawa, K. (1997) Reconstitution, morphology and crystallization of a fatty acid beta-oxidation multienzyme complex from *Pseudomonas fragi*. *Biochem. J. 328* (Pt 3), 815−820.
(32) Tsuchiya, D., Shimizu, N., Ishikawa, M., Suzuki, Y., and Morikawa, K. (2006) Ligand-induced domain rearrangement of fatty acid beta-oxidation multienzyme complex. *Structure. 14*, 237−246.
(33) Pawar, S., and Schulz, H. (1981) The structure of the multienzyme complex of fatty acid oxidation from *Escherichia coli*. *J. Biol. Chem. 256*, 3894−3899.
(34) Campbell, J. W., Morgan-Kiss, R. M., and Cronan, J. E., Jr. (2003) A new *Escherichia coli* metabolic competency: Growth on fatty acids by a novel anaerobic beta-oxidation pathway. *Mol. Microbiol. 47*, 793−805.
(35) Kiema, T., Engel, C. K., Schmitz, W., Filppula, S. A., Wierenga, R. K., and Hiltunen, J. K. (1999) Mutagenic and enzymological studies of the hydratase and isomerase activities of 2-enoyl-CoA hydratase-1. *Biochemistry 38*, 2991−2999.
(36) Yang, S. Y., Bittman, R., and Schulz, H. (1985) Channeling of a beta-oxidation intermediate on the large subunit of the fatty acid oxidation complex from *Escherichia coli*. *J. Biol. Chem. 260*, 2862−2868.
(37) Staack, H., Binstock, J. F., and Schulz, H. (1978) Purification and properties of a pig heart thiolase with broad chain length specificity and comparison of thiolases from pig heart and *Escherichia coli*. *J. Biol. Chem. 253*, 1827−1831.
(38) Battye, T. G. G., Kontogiannis, L., Johnson, O., Powell, H. R., and Leslie, A. G. W. (2011) iMOSFLM: A new graphical interface for diffraction-image processing with MOSFLM. *Acta Crystallogr., Sect. D 67*, 271−281.
(39) Evans, P. (2006) Scaling and assessment of data quality. *Acta Crystallogr., Sect. D 62*, 72−82.
(40) Kabsch, W. (1993) Automatic processing of rotation diffraction data from crystals of initially unknown symmetry and cell constants. *J. Appl. Crystallogr. 26*, 795−800.
(41) McCoy, A. J., Grosse-Kunstleve, R. W., Adams, P. D., Winn, M. D., Storoni, L. C., and Read, R. J. (2007) PHASER crystallographic software. *J. Appl. Crystallogr. 40*, 658−674.
(42) Murshudov, G. N., Vagin, A. A., and Dodson, E. J. (1997) Refinement of macromolecular structures by the maximum-likelihood method. *Acta Crystallogr., Sect. D 53*, 240−255.
(43) Collaborative Computational Project, Number 4. (1994) The CCP4 suite: Programs for protein crystallography. *Acta Crystallogr., Sect. D 50*, 760−763.
(44) Emsley, P., Lohkamp, B., Scott, W. G., and Cowtan, K. (2010) Features and development of coot. *Acta Crystallogr., Sect. D 66*, 486−501.
(45) Chen, V. B., Arendall, W. B., 3rd, Headd, J. J., Keedy, D. A., Immormino, R. M., Kapral, G. J., Murray, L. W., Richardson, J. S., and Richardson, D. C. (2010) MolProbity: All-atom structure validation for macromolecular crystallography. *Acta Crystallogr., Sect. D 66*, 12−21.
(46) Krissinel, E., and Henrick, K. (2007) Inference of macromolecular assemblies from crystalline state. *J. Mol. Biol. 372*, 774−797.
(47) McNicholas, S., Potterton, E., Wilson, K. S., and Noble, M. E. (2011) Presenting your structures: The CCP4mg molecular-graphics software. *Acta Crystallogr., Sect. D 67*, 386−394.
(48) *The PyMOL Molecular Graphics System*, version 1.3r1 (2010) Schrödinger, LLC.

(49) Kabsch, W., and Sander, C. (1983) Dictionary of protein secondary structure: Pattern recognition of hydrogen-bonded and geometrical features. *Biopolymers 22*, 2577−2637.
(50) Altschul, S. F., Gish, W., Miller, W., Myers, E. W., and Lipman, D. J. (1990) Basic local alignment search tool. *J. Mol. Biol. 215*, 403−410.
(51) Huang, Y., Niu, B., Gao, Y., Fu, L., and Li, W. (2010) CD-HIT suite: A web server for clustering and comparing biological sequences. *Bioinformatics 26*, 680−682.
(52) Larkin, M. A., Blackshields, G., Brown, N. P., Chenna, R., McGettigan, P. A., McWilliam, H., Valentin, F., Wallace, I. M., Wilm, A., Lopez, R., Thompson, J. D., Gibson, T. J., and Higgins, D. G. (2007) Clustal W and clustal X version 2.0. *Bioinformatics 23*, 2947−2948.
(53) Page, R. D. (1996) TreeView: An application to display phylogenetic trees on personal computers. *Comput. Appl. Biosci. 12*, 357−358.
(54) Gouet, P., Courcelle, E., Stuart, D. I., and Metoz, F. (1999) ESPript: Analysis of multiple sequence alignments in PostScript. *Bioinformatics 15*, 305−308.